

Analysis of Newtonian and Non-Newtonian Impacts on Acoustic Separation of CTCs

Zahra Taheri¹, Morteza Bayareh^{1*}, Afshin Ahmadi Nadooshan¹

¹ Department of Mechanical Engineering, Shahrekord University, Shahrekord, Iran

ABSTRACT: Metastasis is the main origin of epithelial cancer-based mortality. Since circulating tumor cells (CTCs) are valid biomarkers to diagnose cancer, their isolation and analysis are crucial. Microfluidic technology has experienced remarkable potential to isolate CTCs due to its unique characteristics. The present paper analyzes the influences of Newtonian and non-Newtonian fluids on the continuous separation of CTCs using standing surface acoustic waves (SSAWs). The impacts of inlet velocity, oscillation amplitude, dynamic viscosity, CTC radius, power-law index, and sheath-to-sample flow velocity ratio on the isolation process are examined. The results demonstrate that the separation efficiency declines from 88% to 84% by augmenting the inlet velocity from 1.8 mm/s to 2 mm/s. It is found that for a certain value of CTC radius, the amount of sheath flow velocity can be changed to reach a maximum separation efficiency. Besides, the amount of separation efficiency decreases as the dynamic viscosity of the Newtonian fluid is enhanced and the power-law index of the non-Newtonian fluid is reduced.

KEYWORDS: *Microfluidic technology, SSAWs, CTC, Separation, Non-Newtonian fluid*

INTRODUCTION

Cancer is a disease characterized by the uncontrolled growth of cells, invading nearby tissues, and metastasizing to distant areas of the body. Cancer cells form a tumor by growing, dividing uncontrollably, and accumulating in an area in the body. A number of rare cells from this tumor are aggressive and separated from the primary tumor, shedding in the circulatory system. These cells are called CTCs [1, 2]. Therefore, cell isolation is an essential step in biological research, which is vital to detect the early stages of diseases and to test the effectiveness of drug screening. Cell isolation is used in many fields, including medicine, pharmaceuticals, food production, and environmental issues [3, 4].

In recent years, the emergence of microfluidic technology due to its unique features, including high efficiency and rapid detection, has led to the expansion of cell separation by devices known as microfluidic devices. Microfluidic devices have been a precise and suitable tool for separating CTCs from other blood cells in the last two decades [5]. These devices have specific advantages: low cost, small sample size, portability, high accuracy and sensitivity, ability to integrate several technologies, and short test time for cell separation, classification, and sorting [6]. These devices are divided into two categories: active devices and passive ones. Passive devices do not need external forces and use the force between particles, fluid field, and microchannel structure to separate particles. Some parameters such as inlet flow rate, fluid viscosity, and particle size can be changed to improve separation accuracy. Active separation devices use different external actuators,

such as electric, magnetic, optical, and acoustic fields to separate particles/cells [7]. It can be expressed that in most cases, due to the high efficiency of active techniques, an external energy source is used to separate particles. Passive methods, however, are more suitable from the energy point of view [8]. Sajeesh and Kumar [9] and Dalili et al. [10] discussed the advantages and disadvantages of active and passive techniques for particle separation in microfluidic devices. Among active methods, acoustic-based separation techniques can isolate the cells efficiently with magnificent biocompatibility [11]. Based on experimental observations, CTCs exposed to an acoustic field have more mobility and activity than other blood cells; hence, they concentrate up to a thousand times without affecting their primary function. Thus, CTCs are kept healthy and unchanged during the acoustic isolation process for further assessments [12].

Acoustic waves can be categorized into two groups: bulk acoustic waves (BAWs) and surface acoustic waves (SAWs) [13]. BAWs are excited by placing a composite piezoelectric transducer and influence the entire channel; however, SAWs that are formed along the floor of the channel catch the energy on the surface and exert acoustic radiation force on cells/particles [14]. If SAWs are radiated from interdigital transducers (IDTs), acoustic waves are known as traveling SAWs (TSAWs). SSAWs are created when a pair of IDTs is mounted on the piezoelectric substrate on both sides of the channel, i.e. two TSAWs propagate oppositely [11]. SSAWs are composed of time-averaged pressure nodes and pressure antinodes. The minimum and maximum pressure amplitudes along the SSAWs correspond to the pressure nodes and pressure antinode, respectively.

* Corresponding author's email: m.bayareh@sku.ac.ir
Tel.: +989131081858

Nomenclature

d_0	displacement amplitude, m	p	Pressure, Pa
c_o	Acoustic speed, m/s	Re	Reynolds number
d_c	Cell diameter, m	t	Time, s
f	Frequency, Hz	Greek symbols	
F_{ac}	Acoustic radiation force, N	φ	Acoustic contrast factor
F_D	Drag force, N	μ	Fluid viscosity, Pa.s
k	Wave number	μ_0	Zero shear viscosity, Pa.s
m_c	Mass of cell, kg	μ_∞	Infinite shear viscosity, Pa.s
N	Power-law index	ρ_c	The density of cell, kg/m ³
N_o	The number of cells passing through an outlet	λ	Relaxation time, s
N_T	The total number of cells entering the microchannel	ρ_m	The density of medium, kg/m ³
u	Fluid velocity, m/s	β_c	Cell compressibility
V_o	Inlet velocity, m/s	τ	Stress tensor, Pa

The sign of the acoustic contrast factor, which depends on the density and compressibility of the particle and the medium, determines the acoustic force direction. The positive acoustic contrast factor, which usually exists for solid particles, means that the acoustic radiation force pushes the particles toward the pressure nodes. On the other hand, the negative acoustic contrast factor, which is common for bubbles, leads to their motion towards pressure antinodes. Usually, most solid microparticles and cells cannot be separated due to the sign of acoustic contrast factor, because their acoustic contrast factor has a positive value; hence, microparticles and cells move toward pressure nodes. Therefore, particle/cell separation can be performed based on their size [15, 16], density [17], and compressibility [18] when SSAWs are utilized. It is known that the combined effect of density and compressibility is experienced in the acoustic contrast factor. The role of medium density was demonstrated by Petersson et al. [19].

A common method for separating particles based on SSAWs is to concentrate them along the channel and then expose the particles to the acoustic radiation force. The acoustic field is perpendicular to the flow; thus, the particles move laterally toward the pressure nodes, which are usually in the center of the channel. By adjusting the flow velocity, width, and length of the channel as well as the intensity of the acoustic wave, different particles can be directed toward various outlets. Chen et al. [16] revealed that this technique can separate platelets from whole blood. Lateral displacement of particles becomes more challenging for isolating more than two particles. While they separated all particles utilizing a single microfluidic device [20], some studies employed a multi-stage acoustic field to improve the separation efficiency [21-23].

Based on the size of microparticles, Nam et al. [17] used SSAWs to separate them. Using the hydrodynamic force exerted by the sheath flow, they first concentrated the particles in the center of the channel where the acoustic force is most effective and the shear rate is low. Then, they adjusted the SSAWs so that the pressure nodes were located at the walls and the pressure anti-nodes were placed in the

channel center. They also presented an analytical model, including viscous, acoustic, and diffusion forces to predict particle trajectories. Based on their results, the diffusion effect is insignificant and the practicality of this method to isolate small particles, such as platelets, is acceptable. In another work, they utilized this method to separate platelets from whole blood [24]. The same method was also used to isolate bacteria from blood cells [25] and platelets from whole blood [16].

Recently, Wang et al. [26] examined the influences of microfluidic device angle on the isolation of live cells, including lung and breast cancer cells. They demonstrated that the acoustic contrast factor of these CTCs is different from WBCs by 27.9% and 21.5%, respectively. Qiu et al. [27] employed a hybrid system consisting of an acoustofluidic chip and an ultrasonic transducer to isolate CTCs. They successfully separated 2- μ m agglomerates that were sensitive to the acoustic field. Besides, an acoustoinertial microfluidic device was utilized by Mahboubidoust et al. [28] to isolate CTCs from neutrophils and reached a separation efficiency of 99.3% for breast cancer cells. The optimal particle focusing was achieved when the channel aspect ratio was 0.2 and the flow rate was 2 ml/min.

In previous studies, acoustic separation of microparticles/cells in Newtonian fluid has been examined. In general, whole blood can be considered as a non-Newtonian fluid due to the presence of numerous red blood cells. This paper aims to assess the separation of two types of CTCs, i.e. MCF-7 (breast cancer) cells and HeLa (epithelial cervical cancer), from white and red blood cells by applying an acoustic field. The cells are suspended in Newtonian and non-Newtonian fluids. The present microfluidic device includes two IDTs on the sides of the channel, a sample flow inlet, and two sheath flow inlets. Due to the channel's simplicity and the IDTs' placement, it is possible to fabricate it easily and the findings can be used practically. To the best of the authors' knowledge, the effect of non-Newtonian fluid on the cell separation mechanism has not been analyzed in previous works. In addition, the suspension of cells in a non-Newtonian fluid is more

consistent with reality compared to Newtonian fluids. In the present work, the Carreau model is used to model the non-Newtonian fluid behavior. The value of the power-law index is considered smaller than one; thus, the fluid behaves as a shear-thinning fluid.

Problem Description

The geometry of the problem consists of three parts: piezoelectric substrate, PDMS channel, and IDTs (Fig. 1). To generate SSAWs, a pair of IDTs is mounted on the sides of the PDMS channel on the piezoelectric substrate. The PDMS channel includes the main rectangular channel, inlet channels, and outlet ones. The angle between the sample flow inlet and two sheath flow inlets is 45 degrees. The sheath flow inlets are utilized to control the cell separation process. The outlet includes the middle outlet for the exit of white and red blood cells and the side outlet for the exit of CTCs. The no-slip boundary condition is imposed on the walls and the amount of relative pressure at the outlets is zero. Cells are assumed to be spheres with almost identical physical properties. The characteristics of cells entering the microchannel are presented in Table 1.

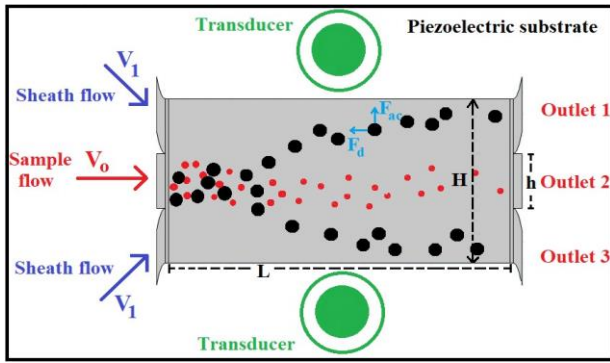


Fig. 1. Schematic of the present problem, where $H = 770 \mu\text{m}$, $h = 257 \mu\text{m}$, and $L = 1500 \mu\text{m}$.

Table 1. Properties of cells.

Cell	Density (kg/m^3)	Average diameter (μm)
WBC	1019	5
RBC	1139	4
HeLa	1018	8
MCF-7	1018	12

Governing equations

Since the channel is considered horizontal, the effects of gravity are negligible. Due to the low values of Reynolds numbers ($Re = \rho V_0 d / \mu < 1$, where V_0 is inlet velocity and μ is dynamic viscosity), the creeping flow regime is considered, meaning that inertial force is very small compared to viscous force. The governing equations for steady incompressible laminar flow of Newtonian or non-Newtonian fluids are continuity and momentum equations:

$$\nabla \cdot \mathbf{u} = 0 \quad (1)$$

$$\rho \frac{D\mathbf{u}}{Dt} = -\nabla p + \nabla \cdot \boldsymbol{\tau} \quad (2)$$

where \mathbf{u} and p are fluid velocity and pressure. $\boldsymbol{\tau} = \mu \dot{\boldsymbol{\gamma}}$ is the stress tensor which is modeled using different non-Newtonian models when the fluid is assumed to be non-Newtonian. In this paper, the Carreau model is used to model non-Newtonian fluid:

$$\mu = \mu_\infty + (\mu_0 - \mu_\infty) \left[1 + (\lambda \dot{\boldsymbol{\gamma}})^2 \right]^{\frac{n-1}{2}} \quad (3)$$

Here, $\mu_0 = 9 \cdot 08 \times 10^{-3} \text{ Pa} \cdot \text{s}$ and $\mu_\infty = 7 \cdot 21 \times 10^{-7} \text{ Pa} \cdot \text{s}$ are the zero shear viscosity and the infinite shear viscosity, respectively, n is the power-law index, and λ is the relaxation time. Also, $\dot{\boldsymbol{\gamma}} = \nabla \mathbf{u} + (\nabla \mathbf{u})^T$ is the fluid strain rate tensor. Except in the section where the effect of n is examined, the power-law index is $n = 0.3568$. The fluid relaxation time has a value of $\lambda = 0.07$.

In order to track the position of the particles inside the microchannel, the cells are injected into the microchannel with an initial velocity equal to the fluid velocity. The forces applied to the cells include drag force (F_D) and acoustic radiation force (F_{ac}). The equation governing the motion of cells follows Newton's second law:

$$\frac{d}{dt}(m_c \mathbf{v}) = F_D + F_{ac} \quad (4)$$

$$F_D = 3\pi d_c \mu (\mathbf{u} - \mathbf{v}) \quad (5)$$

where m_c , \mathbf{v} , and d_c are the mass, velocity, and diameter of cells, respectively.

A pair of IDTs are mounted on the sides of the PDMS channel to generate SSAWs. These waves create F_{ac} on the cells based on their acoustic properties and volume fraction [29]. The amount of F_{ac} is calculated using the following equation [30]:

$$F_{ac} = - \left(\frac{\pi P_o^2 V_c \beta_m}{2\lambda} \right) \varphi(\beta, \rho) \sin(2ky) \quad (6)$$

where P_o , V_c , β_m , k , λ , y , and φ are the acoustic pressure, cell volume, the compressibility of the medium, wave number, wavelength, distance from pressure antinodes on the axis of wave propagation, and acoustic contrast factor, respectively. The wave number is also defined as follows:

$$k = \frac{2\pi f}{c_o} \quad (7)$$

Here, f and c_o are the frequency and acoustic speed in the medium, respectively. The acoustic contrast factor is also obtained utilizing the following equation:

$$\varphi(\beta, \rho) = \frac{5\rho_c - 2\rho_m}{2\rho_c + \rho_m} - \frac{\beta_c}{\beta_m} \quad (8)$$

Here, ρ_c , ρ_m , and β_c are the density of cell, the density of medium, and cell compressibility, respectively.

Finally, by counting the cells in each outlet, the cell separation efficiency can be obtained as follows [31]:

$$\text{Separation Efficiency}(\%) = \frac{N_o}{N_T} \times 100 \quad (9)$$

where N_o and N_T are the number of cells passing through an outlet and the total number of cells entering the microchannel, respectively.

Grid independence test

Triangular elements with an average size of $0.9007 \mu m$ and a minimum size of $0.007729 \mu m$ are used for the grid generation. In order to find a sufficient number of elements and the independence of the solution from the grid, the separation efficiency is calculated in terms of inlet velocity for four different computational grids when $f_0 = 1 MHz$, $R_{CTC} = 12 \mu m$, and $d_0 = 0.08 nm$, where f_0 , R_{CTC} , and d_0 are applied frequency, the radius of CTCs, and displacement amplitude, respectively (Fig. 2). It is demonstrated that there is no noticeable difference in the value of separation efficiency by augmenting the number of elements from 365194 to 512358; therefore, the grid with 365194 elements can be utilized for further simulations. It should be pointed out that the grid study is carried out for Newtonian and non-Newtonian fluids, indicating that the grid with 365194 elements is appropriate for both cases.

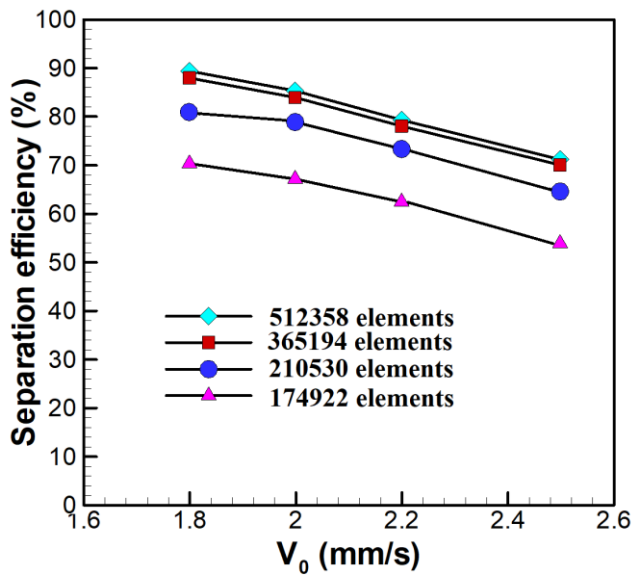


Fig. 2. Separation efficiency versus inlet velocity for different grids when $f_0 = 1 MHz$, $R_{CTC} = 12 \mu m$, and $d_0 = 0.08 nm$.

Validation

To validate the method used in the numerical simulations, the separation efficiency is calculated for different flow rates according to the experimental data reported by Petersson et al. [32] (Fig. 3). They used a frequency of 2 MHz to separate lipid particles from red blood cells in a microchannel with a width of $350 \mu m$, a depth of $125 \mu m$, and a length of 24 mm. This figure indicates a good agreement between numerical and experimental results so that the maximum error is less than 10%. The present simulations assume that the fluid is Newtonian.

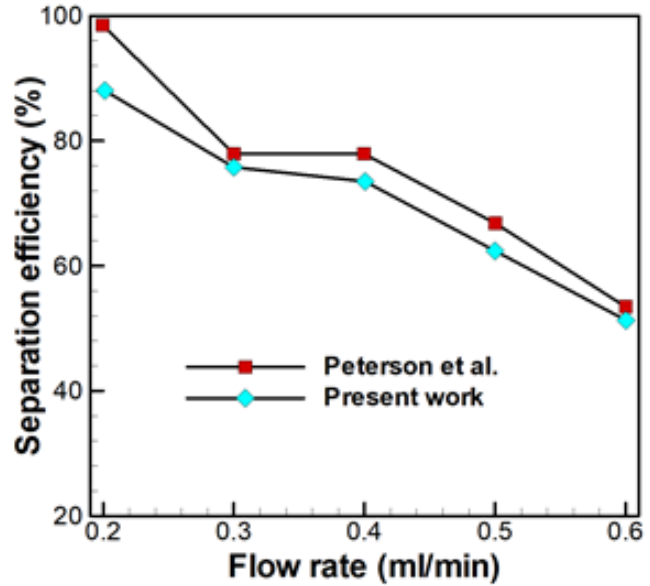


Fig. 3. Separation efficiency in terms of volume flow rate: comparison between the present numerical results and experimental results reported by Petersson et al. [32].

RESULTS

Isolation of CTCs Suspended in Newtonian Fluid

The first stage of the simulations is dedicated to the separation of cells suspended in the Newtonian fluid. Whole blood is considered a non-Newtonian fluid due to the presence of numerous RBCs; however, because the patient's diluted blood sample is used to perform such tests and the number of RBCs per unit volume is reduced significantly, the blood can be assumed as Newtonian fluid. This section evaluates the effect of inlet velocity, fluid viscosity, cell size, the ratio of sheath to main flow velocity, and the amplitude of the acoustic oscillation on the isolation of CTCs.

Effect of inlet velocity

Fig. 4 illustrates the effect of the inlet flow velocity (V_0) on the separation efficiency is examined when the frequency of 1 MHz is applied. As can be seen, by changing the inlet velocity from 1.8 to 2 mm/s, the separation efficiency declines from 88% to 84%. The decrease in efficiency is due to that the CTCs are exposed to the acoustic field for a longer time when the inlet velocity is lower. As a result, the acoustic radiation force overcomes the drag force, leading to more lateral deviation of CTCs. As the lateral deviation of CTCs is augmented, the possibility of them passing through the side outlets is enhanced and the separation efficiency is improved. It should be noted that if the velocity drops below a certain value, it is possible that the CTCs to attach to the channel wall and become trapped. Therefore, for a specific amount of frequency and oscillation amplitude, the optimal velocity for different cell sizes can be determined.

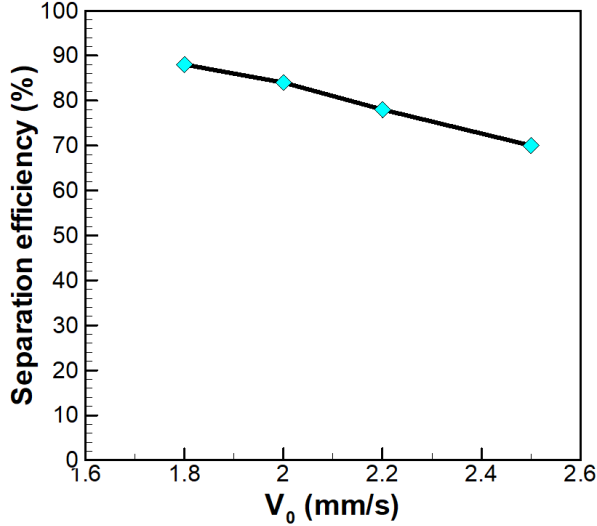


Fig. 4. Separation efficiency as a function of inlet velocity for $f_0 = 1\text{MHz}$, $R_{CTC} = 12\mu\text{m}$, and $d_0 = 0.08\text{nm}$.

The trajectory of cells during the simulation is extracted using the particle tracing module. The present simulations reveal that the trajectory of RBCs and WBCs is almost the same for both Newtonian and non-Newtonian fluids and various effective parameters, including inlet velocity, cell size, and acoustic oscillations, indicating that the blood cells exit from the middle outlet, i.e. outlet 2 (Fig. 5). Fig. 6 depicts the trajectory of CTCs for different inlet velocities, confirming the greater lateral deviation of CTCs as the inlet velocity declines.

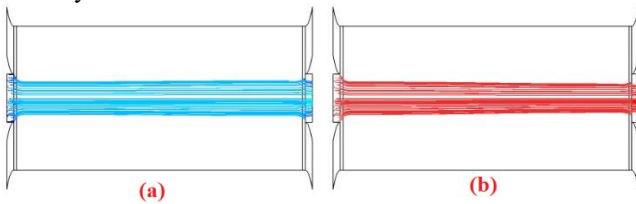


Fig. 5. Trajectory of (a) WBCs and (b) RBCs for Newtonian and non-Newtonian fluids and various values of μ , V_0 , and d_0 when $f_0 = 1\text{MHz}$.

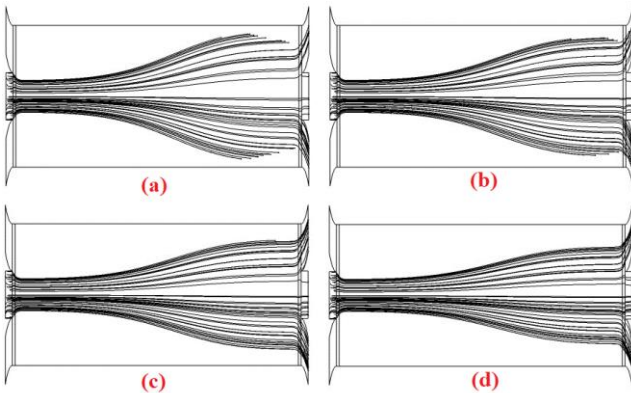


Fig. 6. Trajectory of CTCs in Newtonian fluid for $f_0 = 1\text{MHz}$, $R_{CTC} = 12\mu\text{m}$, $d_0 = 0.08\text{nm}$ when (a) $V_0 = 1.8\text{mm/s}$, (b) $V_0 = 2\text{mm/s}$, (c) $V_0 = 2.2\text{mm/s}$, and (d) $V_0 = 2.5\text{mm/s}$.

Effect of the Ratio of Sheath Flow Velocity to the Sample Flow Velocity

The effect of the ratio of sheath flow velocity to the sample flow velocity (VR) on the separation efficiency of CTCs is shown in Fig. 7a. As can be seen, the separation efficiency is augmented from 36% to 84% by changing VR from 0.5 to 1. This ascending trend is due to that the CTCs located in the vicinity of the walls are exposed to the acoustic force for a longer time due to their lower velocity. Therefore, the influence of the acoustic radiation force on them is greater, resulting in their more lateral deviation so that they are trapped by hitting the channel wall. Thus, the separation efficiency is reduced by varying VR from 0.5 to 1. It can be seen that the separation efficiency declines from 84% to 0% by changing VR from 1 to 2.5. This descending trend is due to the dominance of the inertial force and the less impact of the acoustic radiation force because CTCs experience less lateral deviation and most of them exit the outlet 2. One can conclude that the sheath velocity can be adjusted so that the CTCs are deflected by acoustic radiation force to the extent that they do not collide with the wall. In other words, the optimal sheath velocity can be achieved for different cell sizes. The trajectory of CTCs for two different amounts of VR is illustrated in Figs. 7b and 7c, confirming the above-mentioned conclusions.

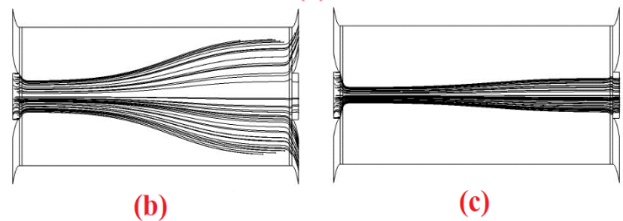
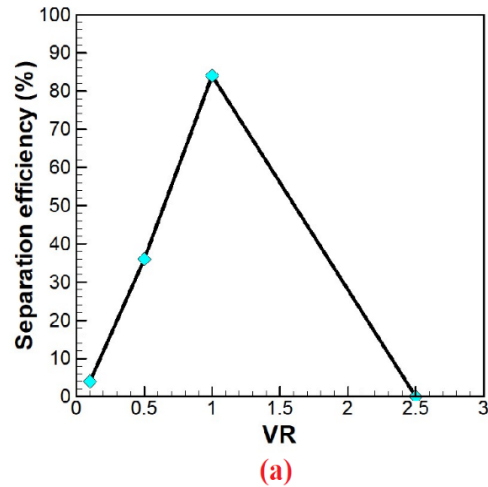
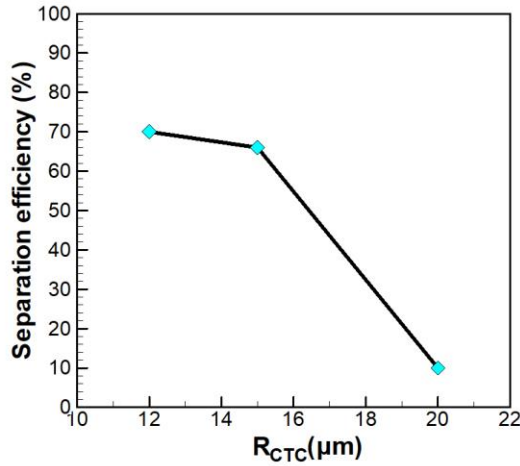


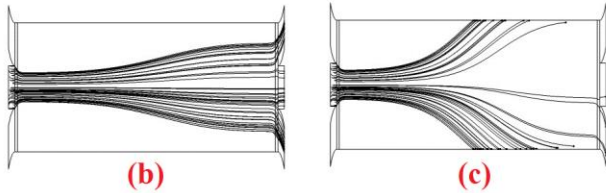
Fig. 7. (a) Separation efficiency in terms of VR , (b) trajectory of CTCs in Newtonian fluid for $VR = 1$, and (c) trajectory of CTCs in Newtonian fluid for $VR = 2.5$ when $f_0 = 1\text{MHz}$, $V_0 = 2\text{mm/s}$, $R_{CTC} = 12\mu\text{m}$, and $d_0 = 0.08\text{nm}$.

Effect of R_{CTC}

The effect of R_{CTC} on separation efficiency is demonstrated in Fig. 8a for $V_0 = 2.5 \text{ mm/s}$ and $d_0 = 0.08 \text{ nm}$. It is observed that the separation efficiency is reduced from 66% to 10% by changing the radius of the CTCs from 15 to 20 μm . According to Eq. 6, the size of the CTCs is directly proportional to the amount of acoustic radiation force acting on them, meaning that the larger the cell size, the more acoustic radiation force and more lateral deviation. Hence, the CTCs collide with the channel walls and do not reach the outlets, i.e. the separation efficiency decreases. Also, for $R_{CTC} = 20 \mu\text{m}$, several simulations are performed (not shown) and the results reveal that the separation efficiency is 28%, 60%, and 88% for the inlet velocities of 3, 4, and 5 mm/s , respectively. It can be concluded that the maximum separation efficiency of CTCs with different sizes corresponds to an optimal inlet velocity. The trajectory of CTCs for two different radii is presented in Figs. 8b and 8c when $V_0 = 2.5 \text{ mm/s}$.



(a)



(b)

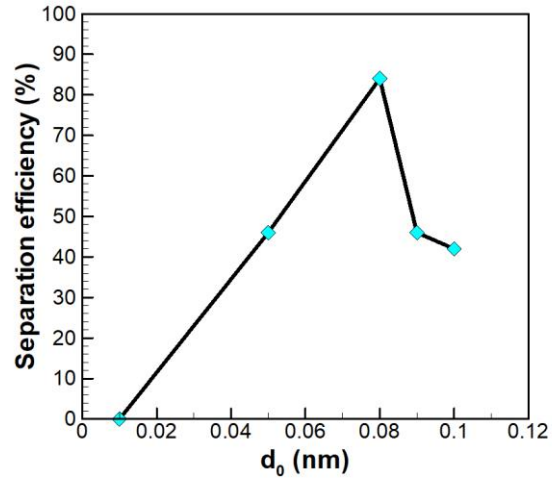
(c)

Fig. 8. (a) Separation efficiency in terms of R_{CTC} , (b) trajectory of CTCs in Newtonian fluid for $R_{CTC} = 12 \mu\text{m}$, and (c) trajectory of CTCs in Newtonian fluid for $R_{CTC} = 20 \mu\text{m}$ when $f_0 = 1 \text{ MHz}$, $V_0 = 2.5 \text{ mm/s}$, $R_{CTC} = 12 \mu\text{m}$, and $d_0 = 0.08 \text{ nm}$.

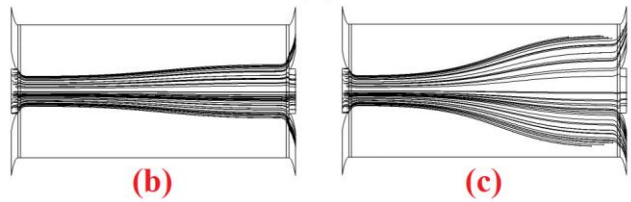
Effect of Acoustic Oscillation Amplitude

Oscillation amplitude (d_0) is the distance of an acoustic particle from the equilibrium state in the medium where the wave propagates. The amount of cell displacement in the flow direction and the lateral direction (perpendicular to the flow) is directly related to the oscillation amplitude. In other words, d_0 only affects the velocity of the particles and does

not affect the flow structure. Since the longitudinal and transverse displacements are dependent on d_0 , it is expected that the value of the lateral deviation and consequently the separation efficiency has an optimal value. Fig. 9a depicts the variations of separation efficiency in terms of d_0 for $f_0 = 1 \text{ MHz}$, $V_0 = 2 \text{ mm/s}$, and $R_{CTC} = 12 \mu\text{m}$. By augmenting the value of d_0 from 0.01 to 0.08 nm , the value of the separation efficiency is enhanced and then reduced. Therefore, $d_0 = 0.08 \text{ nm}$ is chosen as the optimal value. The trajectory of CTCs in Newtonian fluid for two different amounts of d_0 is presented in Figs. 8b and 8c. This figure clearly demonstrates that the amount of longitudinal displacement of particles is much higher than their lateral displacement when $d_0 = 0.01 \text{ nm}$; therefore, all CTCs exit from the middle outlet. By increasing the value of d_0 , the efficiency is improved and reaches a maximum value of 84% when $d_0 = 0.08 \text{ nm}$. Obviously, the optimal value can be different for various frequencies and sizes of CTCs.



(a)



(b)

(c)

Fig. 9. (a) Separation efficiency in terms of d_0 , (b) trajectory of CTCs in Newtonian fluid for $d_0 = 0.01 \text{ nm}$, and (c) trajectory of CTCs in Newtonian fluid for $d_0 = 0.08 \text{ nm}$ when $f_0 = 1 \text{ MHz}$, $V_0 = 2 \text{ mm/s}$, and $R_{CTC} = 12 \mu\text{m}$.

Effect of dynamic viscosity

The effect of fluid dynamic viscosity on the separation efficiency of CTCs is shown in Fig. 10a. With the increase in the dynamic viscosity of the fluid, the separation efficiency is reduced so that the separation efficiency varies from 82% to 60% by enhancing fluid dynamic viscosity from 0.003 to 0.005 $\text{Pa}\cdot\text{s}$. According to Eq. 5, an increment in dynamic viscosity results in an increase in the drag force; thus, the

separation efficiency decreases by reducing the effect of the acoustic force. Figs. 10b and 10c present the trajectory of CTCs in Newtonian fluid for two different dynamic viscosities.

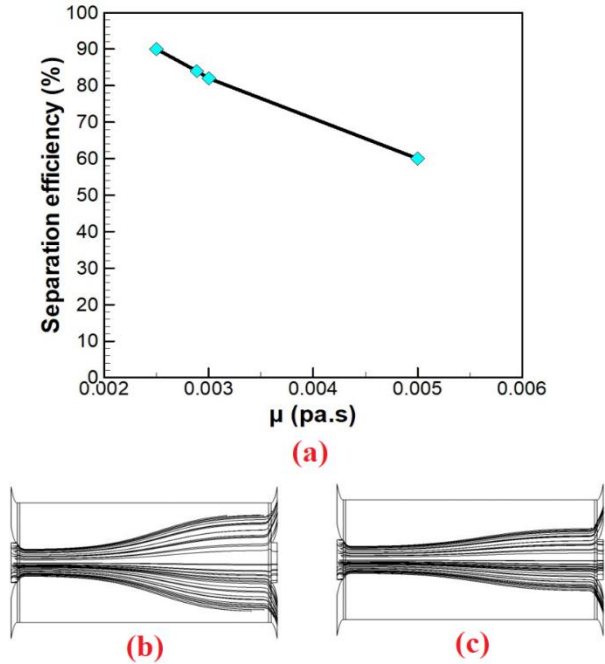


Fig. 10. (a) Separation efficiency in terms of μ , (b) trajectory of CTCs in Newtonian fluid for $\mu = 0.003$ Pa.s, and (c) trajectory of CTCs in Newtonian fluid for $\mu = 0.005$ Pa.s when $f_0 = 1$ MHz, $V_0 = 2$ mm/s, $R_{CTC} = 12$ μ m, and $d_0 = 0.08$ nm.

Isolation of CTCs Suspended in Non-Newtonian Fluid

An average adult has four to six liters of blood in their circulatory system. RBCs, WBCs, and platelets are about 45% of blood volume and the rest belongs to blood plasma. Plasma consists of 90% water and 10% dissolved substances. The number of RBCs is three times the number of WBCs and about ten times more than the number of platelets. As mentioned before, the number of RBCs determines whether the blood behaves as Newtonian or non-Newtonian fluids. Since the process of diluting the patient's blood sample may not be done correctly or the necessary facilities may not be available for it, the assumption that the blood is Newtonian is not correct. On the other hand, the isolation of cells in non-Newtonian fluids using SSAWs can be an interesting subject for investigators. Hence, in this section, numerical simulations are performed by assuming that the blood sample exhibits non-Newtonian behavior. In the present work, the Carreau model is used to model non-Newtonian fluid. The velocity profiles of Newtonian and non-Newtonian shear-thinning fluids in a duct are different in such a way that the distribution of shear-thinning fluid has a smaller maximum value and a wider parabolic profile. When there is no acoustic field, the particles move only under the influence of fluid inertia. Depending on the relative pressure difference between the outlet of the microchannel and the center of the particle, the trajectory of the particle is

determined. Tripathi et al. [33] showed that at very small Reynolds numbers, the drag force on a particle located in a shear-thinning fluid is slightly higher than that in a Newtonian fluid. In shear-thickening fluids, the value of the drag coefficient is slightly lower. Therefore, under the same conditions, it can be concluded that if the CTCs are placed in a non-Newtonian shear-thinning fluid, a greater amount of drag force is applied to them, and as a result, the effect of the acoustic force on their lateral migration is reduced, declining the separation efficiency.

Effect of VR

The effect of VR on the separation efficiency of CTCs is illustrated in Fig. 11a. As mentioned before for the case of Newtonian fluid, the separation efficiency is lower for a lower sheath flow velocity because the CTCs near the wall are exposed to the acoustic radiation force for a longer time and deviate more and may be trapped by colliding with the channel walls. As can be seen, as VR changes from 0.8 to 0.9, the separation efficiency is improved from 76% to 84%. Also, by changing VR from 0.9 to 1, the separation efficiency is reduced from 84% to 76%. The reduction trend is similar to the Newtonian fluid due to the dominance of the inertial force over the acoustic radiation force. Therefore, due to the lower lateral deviation of CTCs, most of them exit from the middle outlet, and the separation efficiency declines. The optimal sheath flow velocity can be estimated for different sizes of CTCs. At an optimal sheath flow velocity, the CTCs do not hit the walls and exit from the side outlets. The trajectory of CTCs in non-Newtonian fluid for different amounts of VR is depicted in Figs. 11b and 11c.

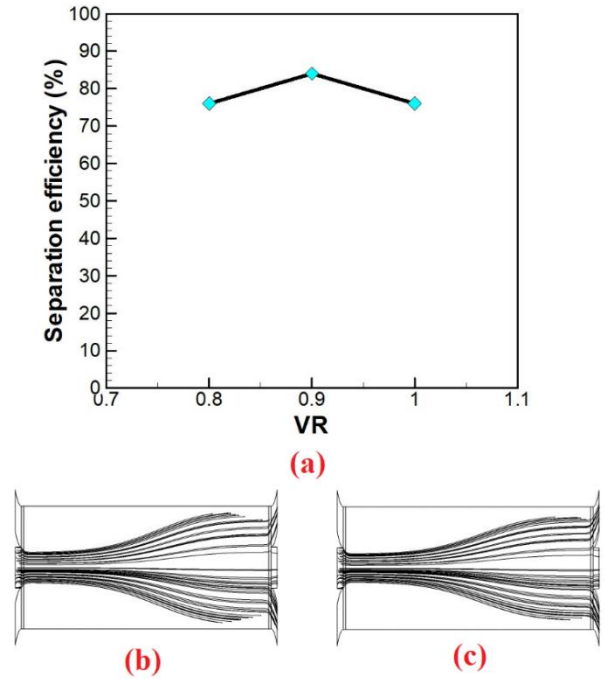


Fig. 11. (a) Separation efficiency versus VR, (b) trajectory of CTCs in non-Newtonian fluid for $VR = 0.9$, and (c) trajectory of CTCs in non-Newtonian fluid for $VR = 1$ when $f_0 = 1$ MHz, $V_0 = 2$ mm/s, $R_{CTC} = 12$ μ m, $d_0 = 0.08$ nm, and $n = 0.3568$.

Effect of R_{CTC}

For the Newtonian fluid, according to Eq. 6, stronger acoustic radiation force is applied to larger CTCs, leading to their more lateral deviation. Hence, they may hit the channel walls and be trapped, resulting in a lower separation efficiency. The effect of CTC radius size in non-Newtonian fluid on separation efficiency is demonstrated in Fig. 12a, indicating that, the separation efficiency is decreased from 76% to 48% by changing the CTC radius from 12 to 15 μm . The trajectory of CTCs is illustrated in Figs. 12b and 12c for two different sizes of CTCs, confirming the quantitative findings.

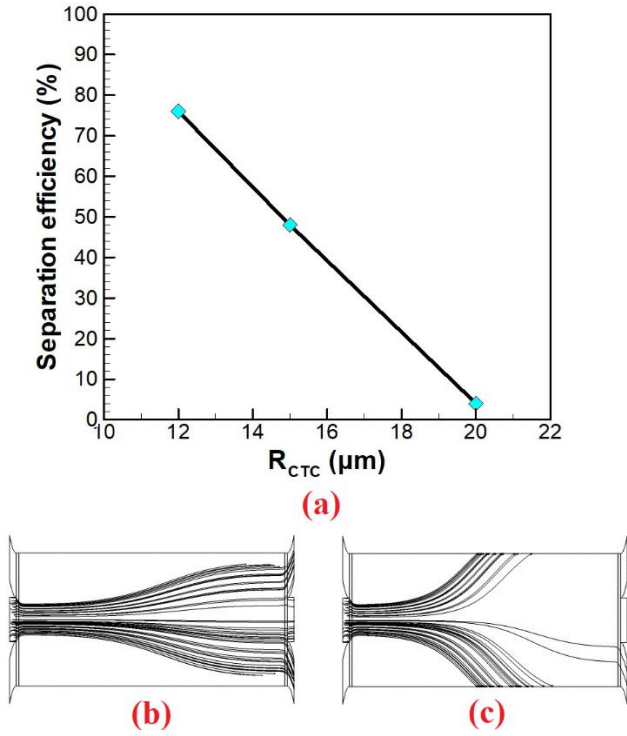


Fig. 12. (a) Separation efficiency as a function of R_{CTC} , (b) trajectory of CTCs in non-Newtonian fluid for $R_{CTC} = 12 \mu\text{m}$, and (c) trajectory of CTCs in non-Newtonian fluid for $R_{CTC} = 20 \mu\text{m}$ when $f_0 = 1\text{MHz}$, $V_0 = 2 \text{mm/s}$, $d_0 = 0.08 \text{nm}$, and $n = 0.3568$.

Effect of Power-Law Index

At very small Reynolds numbers, the drag force in a shear-thinning fluid is slightly higher than that in a Newtonian fluid. Therefore, under the same conditions, if the CTCs are suspended in a non-Newtonian shear-thinning fluid, a stronger drag force is applied to them. As a result, the effect of the acoustic radiation force on the lateral migration of CTCs becomes smaller and the separation efficiency is reduced. Fig. 13a shows the changes in separation efficiency by changing the power-law index. As expected, by reducing n , the separation efficiency declines. The value of the separation efficiency is 76%, 82%, and 84% for $n = 0.3568$, 0.6, and 1, respectively. Figs. 13b and 13c demonstrate the trajectory of CTCs for two values of n . It can be observed

that with the decrease of the deviation from the Newtonian fluid, the amount of lateral displacement of the CTCs is increased and more cells pass through the lateral outlets due to the greater effect of the acoustic radiation force.

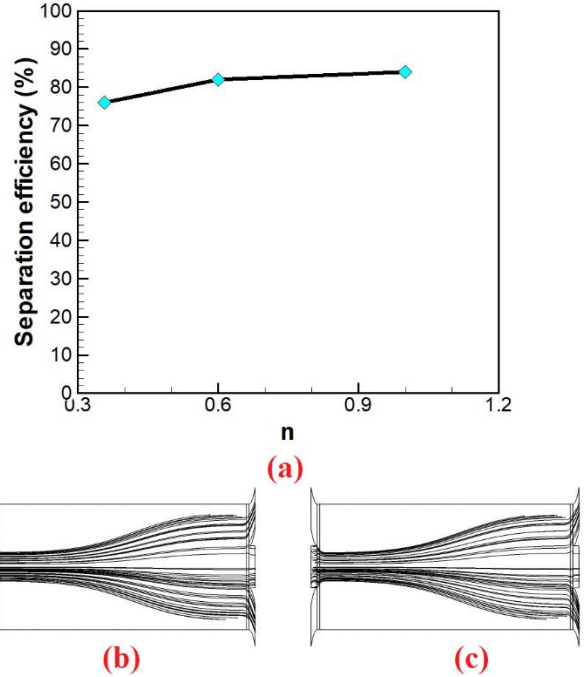


Fig. 13. (a) Separation efficiency as a function of n , (b) trajectory of CTCs in non-Newtonian fluid for $n = 0.3568$, and (c) trajectory of CTCs in non-Newtonian fluid for $n = 1$ when $f_0 = 1\text{MHz}$, $V_0 = 2 \text{mm/s}$, $d_0 = 0.08 \text{nm}$, and $R_{CTC} = 12 \mu\text{m}$.

CONCLUSIONS

In this work, a microfluidic separation device is utilized to isolate CTCs and blood cells using SSAWs. Simulation results demonstrate that a smaller inlet flow velocity leads to a longer time of CTC exposure to acoustic radiation force, a larger lateral deviation, and higher separation efficiency. By changing the inlet velocity from 1.8 to 2 mm/s, the separation efficiency is reduced from 88% to 84%. It is found that the separation efficiency declines from 84% to 0% by changing the amount of VR from 1 to 2.5. The results reveal that the sheath flow velocity, VR, and d_0 can control the deflection of the CTCs in Newtonian and non-Newtonian fluids to achieve maximum separation efficiency. Besides, the separation efficiency is reduced as the dynamic viscosity of the Newtonian fluid is augmented and the power-law index of the non-Newtonian fluid is diminished, indicating that the separation efficiency of CTCs in a Newtonian fluid is greater than that in a non-Newtonian fluid for the same effective parameters. Even though the present microfluidic separation chip has been utilized to isolate CTCs, it can be employed for the effective separation of other biological cells, such as plasma, platelets, etc., to diagnose diseases.

Conflicts of Interest

The authors declare no conflict of interest.

REFERENCES

- [1] Warkiani ME, Khoo BL, Wu L, Tay AKP, Bhagat AA, Han J, Lim C. Ultra-fast, label-free isolation of circulating tumor cells from blood using spiral microfluidics, *Nature Protocols*, 2016;11:134-148.
- [2] Mohammadali R, Bayareh M, Ahmadi Nadooshan A. Numerical investigation on the effects of cell deformability and DLD microfluidic device geometric parameters on the isolation of circulating tumor cells. *Iranian Journal of Chemistry and Chemical Engineering*, 2023, 10.30492/ijcce.2023.1988916.5849
- [3] Bayareh M. Active cell capturing for organ-on-a-chip systems: a review, *Biomedical Engineering*, 2022;67:443-459.
- [4] Mohammadali R, Bayareh M. Deformability-Based Isolation of Circulating Tumor Cells in Spiral Microchannels. *Micromachines*, 2023;14(11):2111.
- [5] Lu C, Xu J, Han J, Li X, Xue N, Li J, Wu W, Sun X, Wang Y, Ouyang Q. A novel microfluidic device integrating focus-separation speed reduction design and trap arrays for high-throughput capture of circulating tumor cells, *Lab Chip*, 2020;20(22): 4094-4105.
- [6] Farahinia A, Zhang W. Numerical analysis of a microfluidic mixer and the effects of different cross-sections and various input angles on its mixing performance, *J. Braz. Soc. Mech. Sci. Eng.*, 2020;42(4):1-18.
- [7] Bayareh M. An updated review on particle separation in passive microfluidic devices, *Chemical Engineering and Processing-Process Intensification*, 2020;153:107984.
- [8] Lenshof A, Laurell T. Continuous separation of cells and particles in microfluidic systems, *Chemical Society Reviews*, 2010;39:1203-1217.
- [9] Sajeesh P, Sen AK. Particle separation and sorting in microfluidic devices: a review, *Microfluidics and Nanofluidics*, 2014;17:1-52.
- [10] Dalili A, Samiei E, Hoorfar M. A review of sorting, separation and isolation of cells and microbeads for biomedical applications: microfluidic approaches, *Analyst*, 2013;144:87-113.
- [11] Shamloo A, Boodaghi M. Design and simulation of a microfluidic device for acoustic cell separation, *Ultrasonics*, 2018;84:234-243.
- [12] Augustsson P, Magnusson C, Lilja H, Laurell T. Acoustophoresis in tumor cell enrichment, *Circulating Tumor Cells: Isolation and Analysis*, 2016:227-248.
- [13] Shields CW, Reyes CD, López GP. Microfluidic cell sorting: a review of the advances in the separation of cells from debulking to rare cell isolation, *Lab Chip*, 2015;15:1230-1249.
- [14] Yeo LY, Friend JR. Surface acoustic wave microfluidics, *Annu. Rev. Fluid Mech.*, 2014;46:379-406.
- [15] Shi J, Huang H, Stratton Z, Huang Y, Huang TJ. Continuous particle separation in a microfluidic channel via standing surface acoustic waves (SSAW), *Lab on a Chip*, 2009;9:3354-3359.
- [16] Chen Y, Wu M, Ren L, Liu J, Whitley PH, Wang L, Huang TJ. High-throughput acoustic separation of platelets from whole blood, *Lab on a Chip*, 2016;16:3466-3472.
- [17] Nam J, Lim H, Kim C, Kang JY, Shin S. Density-dependent separation of encapsulated cells in a microfluidic channel by using a standing surface acoustic wave, *Biomicrofluidics*, 2012;6:024120.
- [18] Gupta S, Feke DL, Manas-Zloczower I. Fractionation of mixed particulate solids according to compressibility using ultrasonic standing wave fields, *Chemical Engineering Science*, 1995;50:3275-3284.
- [19] Petersson F, Åberg L, Swärd-Nilsson A-M, Laurell T. Free Flow Acoustophoresis: Microfluidic-Based Mode of Particle and Cell Separation, *Analytical chemistry*, 2007;79:5117-5123.
- [20] Johnson DA, Feke DL. Adsorptive and membrane-type separators: A biological update, *Separations Technology*, 1995;5:251-258.
- [21] Adams JD, Soh HT. Tunable acoustophoretic band-pass particle sorter, *Applied physics letters*, 2010;97:064103.
- [22] Ding X, Li P, Lin S-CS, Stratton ZS, Nama N, Guo F, Slotcavage D, Mao X, Shi J, Costanzo F. Surface acoustic wave microfluidics, *Lab on a Chip*, 2013;13:3626-3649.
- [23] Ding X, Peng Z, Lin S-CS, Geri M, Li S, Li P, Chen Y, Dao M, Suresh S, Huang TJ. Cell separation using tilted-angle standing surface acoustic waves, *Proceedings of the National Academy of Sciences*, 2014;111:12992-12997.
- [24] Destgeer G, Alazzam A, Sung HJ. Continuous separation of particles in a PDMS microfluidic channel via travelling surface acoustic waves (TSAW), *Journal of Mechanical Science and Technology*, 2016;30:3945-3952.
- [25] Destgeer G, Ha BH, Jung JH, Sung HJ. Submicron separation of microspheres via travelling surface acoustic waves, *Lab on a Chip*, 2014;14:4665-4672.
- [26] Wang H, Boardman J, Zhang X, Sun C, Cai M, Wei J, Dong Z, Feng M, Liang D, Hu S, Qian Y, Dong S, Fu Y, Torun H, Clayton A, Wu Z, Xie Z, Yang X. An enhanced tilted-angle acoustic tweezer for mechanical phenotyping of cancer cells, *Analytica Chimica Acta*, 2023;1255:341120.
- [27] Qiu H, Wang H, Yang X, Huo F. High performance isolation of circulating tumor cells by acoustofluidic chip coupled with ultrasonic concentrated energy transducer, *Colloids and Surfaces B: Biointerfaces*, 2023;222:113138.
- [28] Mahboubidoust A, Heidari Velisi A, Ramiar A, Mosharafi H. Development of a hybrid acousto-inertial microfluidic platform for the separation of CTCs from

- neutrophil, *European Journal of Mechanics - B/Fluids*, 2023;99:57-73.
- [29] Schmid L, Weitz DA, Franke T. Sorting drops and cells with acoustics: acoustic microfluidic fluorescence-activated cell sorter, *Lab on a Chip*, 2014;14:3710-3718.
- [30] Lenshof A, Magnusson C, Laurell T. Acoustofluidics 8: Applications of acoustophoresis in continuous flow microsystems, *Lab on a Chip*, 2012;12:1210-1223.
- [31] Shiriny A, Bayareh M. On magnetophoretic separation of blood cells using Halbach array of magnets, *Meccanica*, 2020;55:1-14.
- [32] Petersson F, Nilsson A, Holm C, Jönsson H, Laurell T. Separation of Lipids from Blood Utilizing Ultrasonic Standing Waves in Microfluidic Channels, *The Royal Society of Chemistry*, 2004;129:938-943.
- [33] Tripathi A, Chhabra RP, Sundararajan T. Power law fluid flow over spheroidal particles, *Industrial & Engineering Chemistry Research*, 1994;33(2):403-410.